

Kinematics and Origin of Gas in the Disk Galaxy NGC 2655

O.K. Silchenko¹, A.V. Moiseev^{2,1}, A.S. Gusev¹, and D.V. Kozlova³

Sternberg Astronomical Institute of the Lomonosov Moscow State University, Moscow, Russia¹

Special Astrophysical Observatory of the Russian Academy of Sciences, Nizhnij Arkhyz, Russia²

Leibniz-Institut für Astrophysik (AIP), Ander Sternwarte 16, 14482 Potsdam, Germany³

The new observational data concerning distribution, excitation, and kinematics of the ionized gas in the giant early-type disk galaxy NGC 2655 obtained at the 6m telescope of the Special Astrophysical Observatory (SAO RAS) and at the 2.5m telescope of the Caucasian Mountain Observatory (CMO SAI MSU) are presented in this work. The joint analysis of these and earlier spectral observations has allowed us to make a conclusion about multiple nature of the gas in NGC 2655. Together with a proper large gaseous disk experiencing regular circular rotation in the equatorial plane of the stellar potential of the galaxy for billions years, we observe also remnants of a merged small satellite having striked the central part of NGC 2655 almost vertically for some 10 million years ago.

Keywords: *galaxies: early-type—galaxies: evolution—galaxies: starformation—galaxies: individual: NGC 2655*

1 INTRODUCTION

The morphological type of lenticular galaxies was introduced by Hubble (1936) as a transitional type between ellipticals and spirals. However, having a large-scale stellar disk in their structure, lenticulars did not show noticeable star formation in it, opposite to spirals. It is very early that a hypothesis was proposed that star formation does not occur in the disks of lenticular galaxies, because there is no gas there; and S0s have no gas, because it was somehow "removed", for example, by interaction with hot intergalactic medium in a cluster (Gunn and Gott, 1972; Larson et al., 1980). However, since then the paradigm of the spiral (disk) galaxy evolution has changed since then, it became clear that the entire evolution of disk galaxies is governed by an inflow of cold gas from outside compensating for any losses of it in the disk, in particular, the losses due to star formation (Tacconi et al., 2020). Also, deep radio observations, both large-scale surveys like ALFALFA (Grossi et al., 2009) and targeted studies of specific samples of early-type galaxies, such as the ATLAS-3D survey (Serra et al., 2012), showed that almost half of the field lenticular galaxies has massive extended gaseous disks. Why does not the same star formation take place in these disks as that in the disks of spiral galaxies?

Observations of gas kinematics in field lenticular galaxies have always shown impressive fraction of decoupled rotation of gas and stars – from 24% (Kuijken et al., 1996) in earlier long-slit studies up to 36% (Davis et al., 2011) and even up to half of all lenticular galaxies in the extremely sparse environment (Katkov et al., 2015). We have previously concluded (Silchenko et al. 2019) that the suppressed star formation in gas-rich lenticular galaxies may be due to the off-plane inflow of the accretion flow: the gas falling into the potential well of the stellar disk suffers shocks, is heated, and becomes unable to form stars. We tested this hypothesis with a sample of 18 lenticular galaxies having extended gaseous disks, by observing them through panoramic spectroscopy, with the Fabry-Perot scanning interferometer of the 6m SAO RAS telescope. We have constructed 2D line-of-sight velocity distributions and have

traced the orientation of the gas rotation plane in space along the galactic radius. Indeed, star formation (particularly the star formation rings in lenticular galaxies) appeared to locate only at the radii, where the gas lies onto the plane of the stellar disk. On the contrary, in inclined gaseous disks, star formation does not proceed (Silchenko et al., 2019). One of the targets in our sample in this work was a nearby giant lenticular galaxy NGC 2655. Figure 1 presents its images provided by the ground-based photometric observations taken from the BASS survey and by high spatial resolution composite observations from the Hubble Space Telescope.

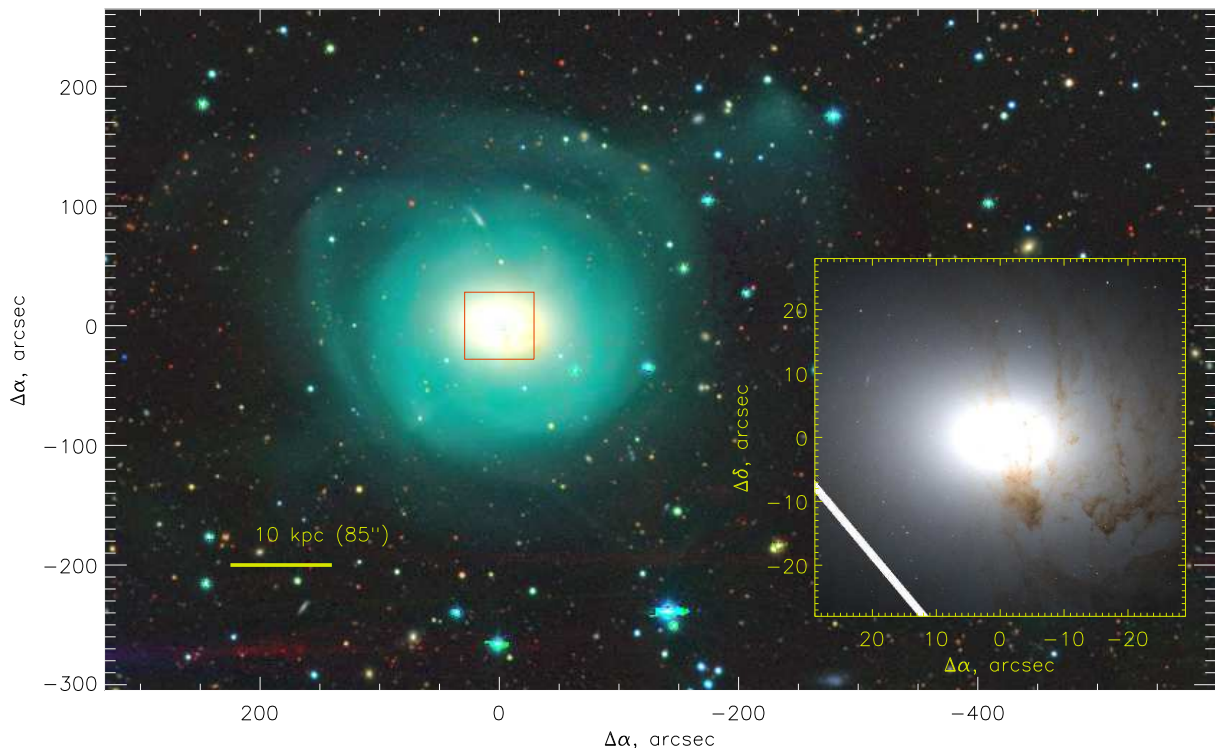


Figure 1: The images of NGC 2655 in composite colors: *the left plot* – the deep broad-band image of the galaxy taken from the DESI Legacy Imaging Surveys resource (Dey et al. 2019), *the right plot* – the image of the central part of the galaxy obtained in broad-band filters by the Hubble Space Telescope. At the *the right plot* one can see asymmetric dust rings produced by the projection of the circumnuclear polar disk.

NGC 2655 is a giant disk galaxy in the center of a group: at a currently accepted distance

to the galaxy of 24.4 Mpc (the scale is 118 pc/arcsec), its absolute magnitude is $M_K = -25$ (LEDA and NED), and the mass of the stellar population is $2 \cdot 10^{11}$ solar masses (Bouquin et al., 2018). The group includes seven galaxies brighter than $M_B = -15$, all of them are of the late type (Garcia 1993). With this configuration, one would expect that the whole gas content of NGC 2655 could result from accumulating the surrounding dwarfs by the central galaxy. Indeed, NGC 2655 is abundant in neutral hydrogen: according to the earliest surveys, up to 3–6 billion solar masses of neutral hydrogen have been found in the galaxy (Lewis and Davies, 1973). It forms a giant disk with a diameter of five times the diameter of the stellar disk (Huchtmeier and Richter, 1982). The integrated star formation rate (SFR) estimated from the ultraviolet fluxes of the galaxy according to the data produced by the GALEX space telescope is 0.08 solar masses per year (Bouquin et al., 2018), which places the galaxy significantly below the Main Sequence classifying it as a "galaxy with quenched star formation" (Cortese et al. 2020). At the same time, it should be noted that such SFR is anomalously low for the observed abundance of H I (Catinella et al. 2018). Detailed investigation of the spatial distribution of the neutral hydrogen density (Shane and Krumm 1983, Sparke et al. 2008) reveals the extension of the gaseous disk in a position angle of $\sim 110^\circ$; we are going to compare this orientation with the parameters of the orientation of the stellar disk in Discussion in the present paper. As for the kinematics of the stars and gas, mapped for the central part of the galaxy through the panoramic spectroscopy, the gas demonstrates a polar rotation in the center with respect to the stars (Silchenko and Afanasiev, 2004; Dumas et al., 2007).

Another feature which is worth to be taken into account is the active nucleus of NGC 2655. Most researchers consider the nucleus of NGC 2655 as a Seyfert type II following our conclusion (Silchenko and Burenkov, 1990); but, for example, Keel and Hummel (1988) noted a strong emission line $[\text{OI}]\lambda 6300$ in the nucleus spectrum and classified it as a LINER. The NGC 2655 nucleus reveals a noticeable flux in X-ray including hard X-ray range (Terashima et al., 2002). High-resolution mapping of the NGC 2655 nucleus in the radio continuum detects

a source with a steep spectrum which is compact both at wavelengths of 6 cm and 20 cm (Hummel et al., 1984); and from the nucleus a jet comes out in the west-east direction, which curves farther from the nucleus to the north-south direction (Ho and Ulvestad, 2001). Perhaps it is the jet that excites another compact radio source, at 15'' (1.7 kpc) to the south-east from the nucleus, which demonstrates the same steep spectrum as the nucleus (Keel and Hummel, 1988).

NGC 2655 is a testbed case of highly inclined rotation of gas in the absence of any star formation in a gas-rich S0, which is of particular interest for us. However, the large-scale pattern of the velocity distribution in the extended gaseous disk of NGC 2655 cannot be understood within a simple geometric model of a flat inclined rotation plane. Both the velocities and the brightness distribution of the emission lines in this galaxy reveal a very complex pattern. We have undertaken some additional observations and are now ready to look into the details of how and when the gas has come to NGC 2655.

2 NEW OBSERVATIONS

We have already devoted several papers to the galaxy NGC 2655 (Silchenko and Burenkov, 1990; Silchenko and Afanasiev, 2004; Silchenko et al., 2019), and we have since a tremendous collection of the spectroscopic data obtained earlier with the 6-m BTA telescope. However, some incomprehensible moments remained in the interpretation of the ionized gas kinematics and, in order to clarify the whole picture, we decided to obtain additionally data.

2.1 Mapping in Emission Lines

We obtained an image of the galaxy with the NBI camera (Shatsky et al., 2020) in a narrow Halp filter centered onto the complex of bright ionized-gas emission lines $H\alpha + [NII]\lambda\lambda 6548, 6583$, having the transition peak at 656 nm, with the 2.5-m telescope of the Caucasus Mountain Observatory of SAI MSU (Shatsky et al., 2020) on January 10, 2018. The seeing during the

observations was $2.5''$. The center wavelength of the filter used was 6560 \AA , the bandwidth was 77 \AA , so both the $[\text{NII}]\lambda\lambda 6548, 6583$ doublet lines and the hydrogen Balmer line $\text{H}\alpha$ fell there. At the same time, a feature of NGC 2655 is that the $[\text{NII}]\lambda 6583$ line is stronger than the $\text{H}\alpha$ line everywhere through the body of the galaxy (Silchenko and Burenkov, 1990). The total exposure of the galaxy image obtained in the emission lines was 25 minutes. The image scale was $0.155''$ per pixel. In addition to photometry in the narrow Halp filter, the galaxy was also exposed in the neighboring continuum for 20 minutes (through the filter with a width of 100 \AA centered on 6430 \AA), so that after subtracting the image in the continuum from the image obtained in the Halp filter, it would be possible to obtain a proper intensity distribution of the emission lines. Figure 2 shows the result of this procedure together with the color map calculated from the broadband photometry in the BASS survey (taken from the Legacy Survey resource, Dey et al. 2019). The morphology of the image in the emission lines represents a narrow loop, the center of which does not coincide with the center of the galaxy, plus a compact emission-line region to south-east from the nucleus, which was previously detected in radiocontinuum emission (indicated in our picture as ESE). A red (dusty) loop outlines the inner edge of the gas emission loop and is especially bright to the south of the center of NGC 2655. It is apparently associated with shock fronts generated by the collision of the polar nuclear gaseous disk with proper gas of the galaxy, probably lying in the main plane of the galactic disk.

2.2 Long-slit Spectroscopy

Additional long-slit spectroscopic data were obtained on May 26, 2022, at the BTA, the 6m SAO RAS telescope, with the SCORPIO-2 multi-mode focal reducer (Afanasiev and Moiseev, 2011). The VPHG1200@540 grism was used with a sensitivity maximum at 5400 \AA providing the full optical range of spectroscopic observations in the wavelength range of $3650\text{--}7300 \text{ \AA}$ with a resolution of about 5 \AA . The slit was posed in two position angles: to include the "radio loud" ESE compact emission region (Fig. 2) and to catch the top of the northern part of the

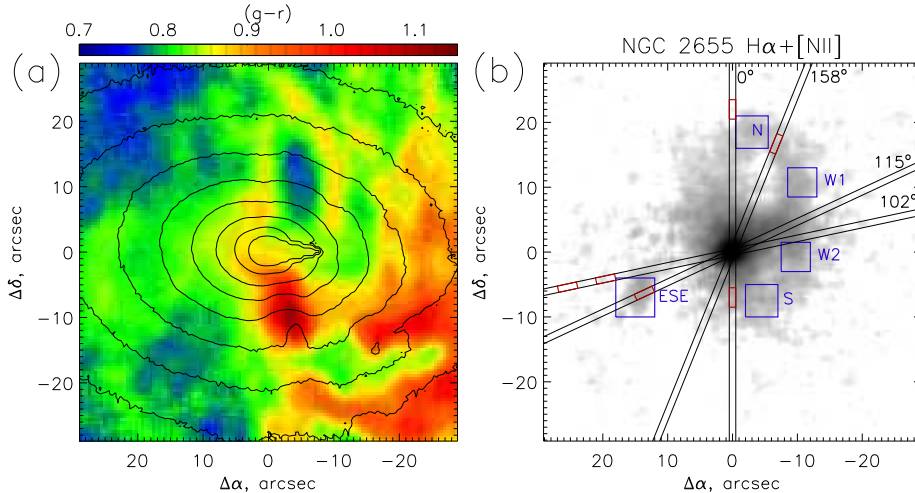


Figure 2: The central part of NGC 2655: *the left plot* – the $g - r$ color image derived from the data of the BASS survey, *the right plot* – the image through the narrow-band filter $H\alpha + [NII]$, which includes the emission lines $H\alpha + [NII] \lambda\lambda 6548, 6583$, according to our data obtained at the 2.5m telescope of CMO SAI MSU, after continuum subtracting. Some particular regions seen in the emission lines are marked for further spectral analysis and discussion.

circumnuclear emission loop; the exposure times were 1600 sec and 800 sec respectively. The seeing quality during the spectroscopic observations in 2022 was $2.4''$. These long-slit cross-sections, together with the cross-sections at the position angles of $PA = 102^\circ$ and $PA = 0^\circ$, previously obtained with the same instrument and the same grism, were used to measure the fluxes of various emission lines and their ratios for the selected regions at different distances from the center of the galaxy, and also to trace the line-of-sight velocities of the gas and the stars.

3 EXCITATION OF THE IONIZED GAS

Previously it was noted more than once (e.g., Sil'chenko and Burenkov 1990, Keel and Hummel 1988) that the strong emission lines in the spectrum of the NGC 2655 nucleus show flux ratios characteristic of a Seyfert type II active nucleus or a LINER one. Moreover, Keel and Hummel

(1988), analyzing their spectrum of the ESE clump, modest as concerning the spectral range and the S/N ratio, have suspected that the spectrum of the ESE clump which is located in 1.8 kpc from the nucleus, is very similar to the nuclear spectrum in terms of the pattern of line flux ratios. Since the limitations on the energy of the nucleus did not allow explaining the ionized gas of the ESE clump as excited by the radiation of the central engine of the active nucleus, it was proposed that the gas excitation source here is a shock wave from the active nucleus jet which, according to radio interferometry, seems to be directed at the appropriate position angle.

We obtained rather deep spectra with the 6-m BTA telescope at four different slit orientations. Measurements of the flux ratios of the emission lines in these four spectra showed that the characteristic flux ratio dominated by the highly-excited [OIII] λ 5007 line is observed throughout the disk of NGC 2655, not only in the ESE clump but also in the polar central loop (clumps N, W1, and S), and in the regular gaseous disk of NGC 2655 up to the distance of 8 kpc from the center. Figure 3 shows the diagnostic diagrams – the so called BPT-diagrams proposed by Baldwin et al. (1981) for diagnosing a gas ionization source – to compare the ratio of the high-excitation [OIII] λ 5007 line to the nearest Balmer hydrogen line $H\beta$, and the ratio of the low-excitation [NII] λ 6583 line to the neighboring Balmer hydrogen line $H\alpha$, for some selected areas of NGC 2655. The red dotted and green dashed lines separate the area of the emission regions excited by young stars (to the left and below the line) from other excitation mechanisms, according to the papers by Kauffmann et al. (2003) and Kewley et al. (2001) respectively. Other excitation mechanisms are the ionization either by the power-law spectrum of the active nucleus or by a shock wave: the BPT-diagram does not makes it possible to distinguish between these two mechanisms. Since the regions under study are located at different distances from the active nucleus, from 1 to 8 kpc, and the line ratios are similar for all them, we think that we are dealing with gas excitation by a shock wave. Seven of the eight regions studied contain the gas likely excited by shock wave. Although the areas of excitation by shock

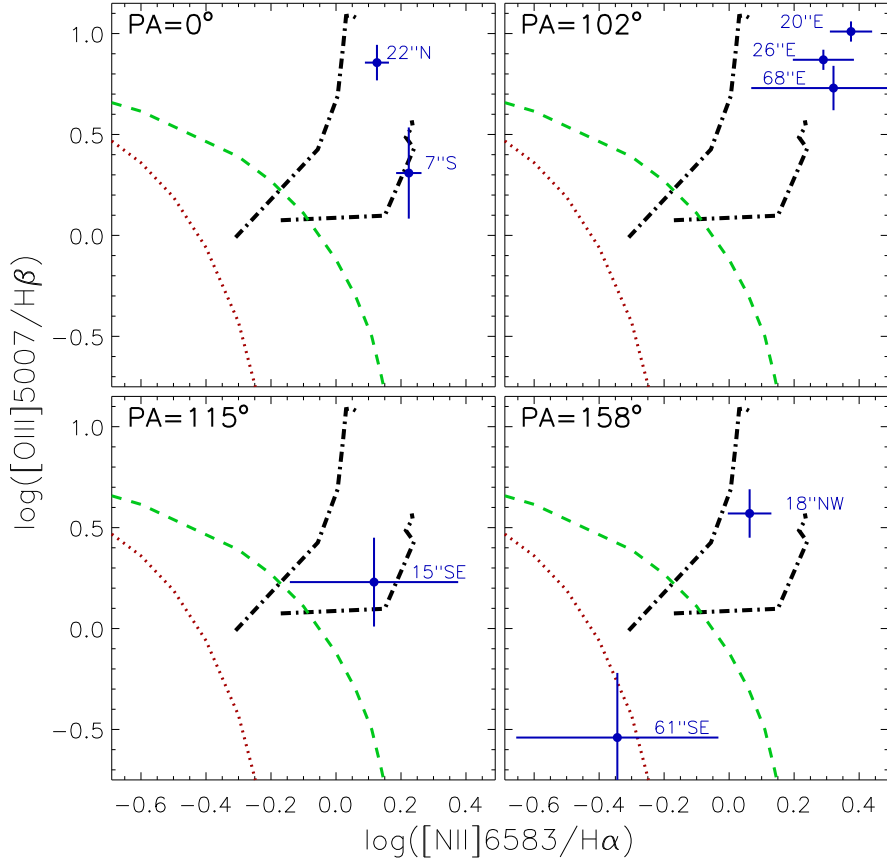


Figure 3: The diagnostic BPT-diagrams to determine a ionized-gas excitation source presented for four long-slit cross-sections of NGC 2655. The slit PA s are indicated in the upper left corner of each plot, the distance from the center (and the direction along the slit, north or south, east or west) are given for every point (emission-line region). The dotted red line and the green dashed line separate the areas for emission regions excited by young stars (to the left and down) and other excitation mechanisms according to Kauffmann et al. (2003) and Kewley et al. (2001), respectively. The dashed-dot fat lines show the models of shock excitation for the gas with solar metallicity and the typical electronic density of $n = 1 \text{ cm}^{-3}$ according to Allen et al. (2008). Along every model broken line the shock velocity rises from bottom to top, from 200 km/s to 1000 km/s; the right broken line corresponds to the shock wave propagating in low-density environment, and the left one – to the shock model with precursor.

waves and by a Seyfert nucleus overlap in the BPT-diagrams, in this case we are talking about the gas excitation at a large distance from the center, and already Keel and Hummel (1988) have estimated that the radiation from the active nucleus of NGC 2655 is not enough even to excite the ESE region at $15''$ from the center, not to mention more distant regions. At the orientation $PA = 102^\circ$ one can see how the shock wave slows down with distance from the center: if we compare the line ratios measured by us with the Allen et al. (2008) models, then from the point $r = 20''$ to the point $r = 60''$, the velocity of the shock wave falls down by some 150 km/s. Only a single region, at 7 kpc south of the center in $PA = 158^\circ$, is excited by young stars. This compact region is located at the periphery of the outer disk and is also visible in the ultraviolet (Fig. 4). Since the gas in this region is ionized by young stars, we can estimate its metallicity from the strong-line flux ratios calibrated using the HII region spectra modeled in detail. We used two popular sources of such calibrations and obtained estimates for the oxygen abundance in the outer gas for NGC 2655: $12 + \log(\text{O}/\text{H}) = 8.58 \pm 0.18$ dex by the indicator N2 and $12 + \log(\text{O}/\text{H}) = 8.58 \pm 0.16$ dex by the indicator O3N2 (Marino et al. 2013), or $12 + \log(\text{O}/\text{H}) = 8.71 \pm 0.18$ dex by the indicator N2 and $12 + \log(\text{O}/\text{H}) = 8.79 \pm 0.21$ dex by the indicator O3N2 (Pettini and Pagel, 2004). Despite the low accuracy of these estimates, we can still confirm that the metallicity of the gas is approximately solar, and this is at the periphery of the galaxy disk!

4 THE DETAILED GAS KINEMATICS

Earlier, we noted more than once the polar rotation of the ionized gas in the central region of NGC 2655 (Silchenko and Afanasiev, 2004; Silchenko et al., 2019). However the actual pattern of gas kinematics throughout the entire galaxy can be much more complicated than simply warped rotation plane. The neutral hydrogen outside the stellar disk rotates regularly, in a circular manner according to the apparent orientation of the HI disk, with a kinematical major axis close to $PA = 110^\circ$; Sparke et al. (2008) proposed a model with a smooth turn of

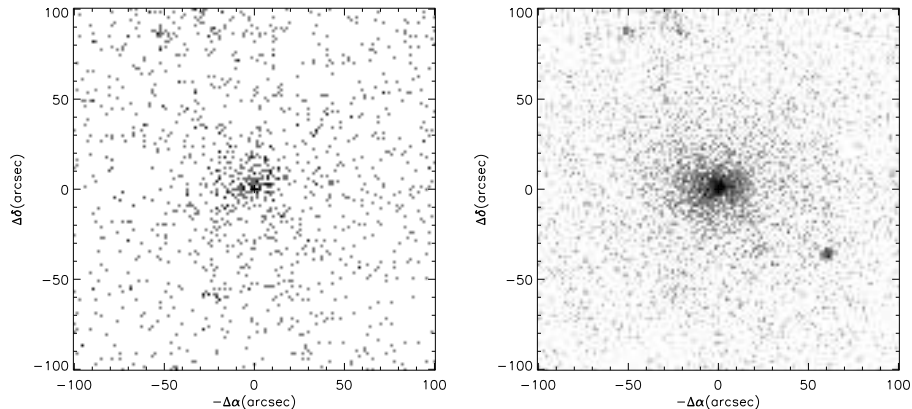


Figure 4: The ultraviolet maps of NGC 2655 according to the GALEX data: *the left* – the FUV map, $\lambda \approx 1500 \text{ \AA}$, *it the right* – the NUV map, $\lambda \approx 2300 \text{ \AA}$.

the gaseous disk when going toward the center of the galaxy. Our data on the ionized gas in the outermost regions of the disk, at $R > 40''$, also seem to agree with the stellar kinematics (Silchenko et al., 2019). However, a lot of details in the distribution of the emission-line surface brightness in Fig. 2 rather indicates not a smooth warp of the gaseous disk but the presence of several gas subsystems with different kinematics at the line of sight. This last hypothesis is also consistent with the shock excitation of the gas throughout the disk of NGC 2655.

Using the benefit of rather high spectral resolution of our data obtained with the Fabry-Perot scanning interferometer, as a second step of our analysis of these data, we decided to take a closer look at the line profiles; the line analyzed is the $[\text{OIII}]\lambda 5007$ emission line scanned in the narrow spectral range over the entire body of NGC 2655 with the Fabry-Perot interferometer (FPI). The line profiles appeared to be complex and multi-component. Figure 5 presents the examples of the Gaussian line fitting for the loop areas marked as N, W1, W2, and S in Fig. 2. Let us note that although the FPI instrumental profile differs from the pure Gaussian one and can be rather described by a Voigt profile, but in the case of the given FPI, the observed line profiles differ little from the Gaussian one which can be clearly seen in Fig. 5.2. In every region

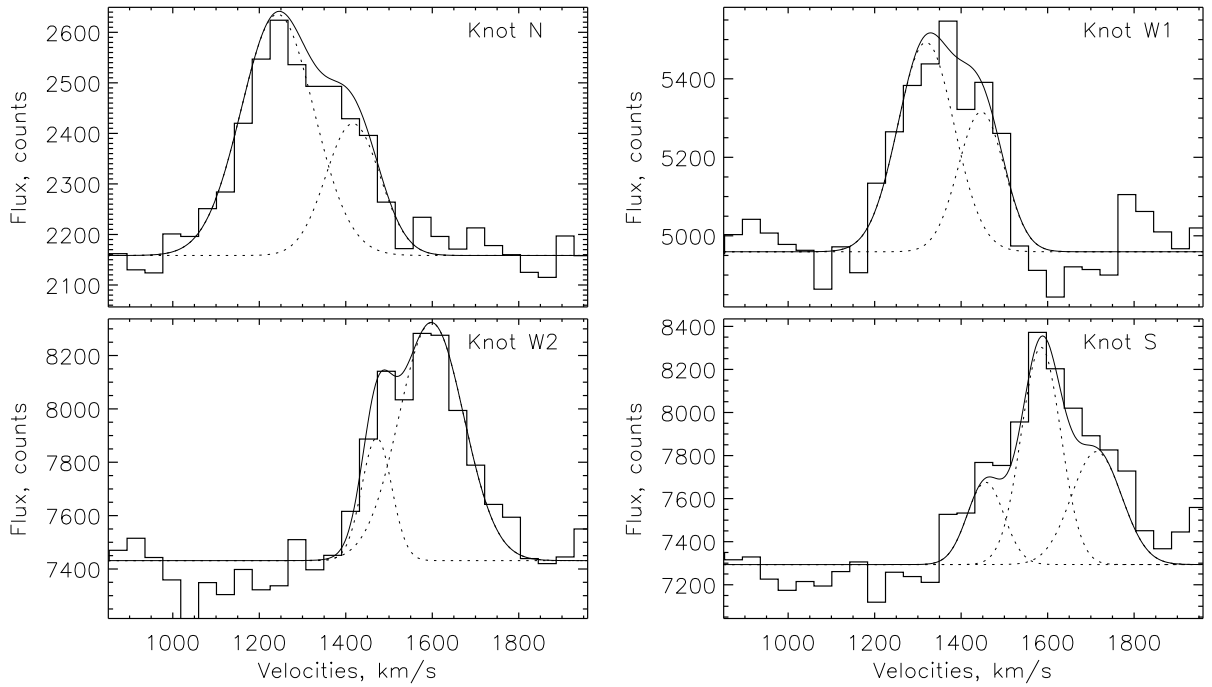


Figure 5: The Gauss-analysis of the $[\text{OIII}]\lambda 5007$ emission-line profiles for the compact emission-line regions designated in Fig. 2 as N (the upper left), W1 (the upper right), W2 (the bottom left), and S (the bottom right). The three former regions reveal the presence of two velocity components at the line of sight each: 1196 ± 12 km/s and 1371 ± 16 km/s (N), 1273 ± 33 km/s and 1401 ± 37 km/s (W1), 1560 ± 6 km/s and 1431 ± 6 km/s (W2), respectively. The southern loop clump reveals three velocity components, 1539 ± 11 km/s, 1667 ± 32 km/s, and 1371 ± 16 km/s.

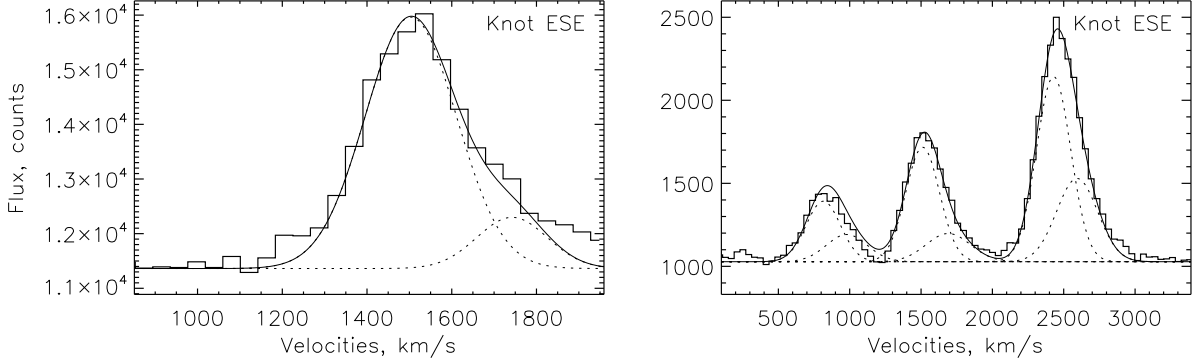


Figure 6: The Gauss-analysis of the emission-line profiles for the clump ESE: the $[\text{OIII}]\lambda 5007$ line has the velocity components 1499 ± 99 km/s and 1737 ± 377 km/s, according to the Fabry-Perot data analysis; and the long-slit data gives 1517 ± 35 km/s and 1730 ± 295 km/s for the $\text{H}\alpha$ profile, and 1490 ± 36 km/s and 1677 ± 138 km/s for the nitrogen doublet profile.

N, W1, W2, and S, we can distinguish at least two components with different line-of-sight velocities. In the N and S regions, the stronger components imply the polar rotation of the loop; but there are also weaker components demonstrating line-of-sight velocities close to the systemic velocity of the galaxy, 1400 km/s, that is expected for the gas at the minor axis of the disk. Obviously, the weak components belong to the gaseous disk rotating in the plane of the stellar disk, whose isophote major axis (and the line of nodes) is aligned close to the west-east direction.

For the radio-loud ESE emission region located at 1.8 kpc southeast of the nucleus, Fig. 6 shows the results of the Gaussian fitting for three lines: for the oxygen line derived from the Fabry-Perot data and for the hydrogen $\text{H}\alpha$ and the nitrogen doublet according to the long-slit spectroscopy data. Although the weak component is measured here with low accuracy, but for all three elements it occurs that in the ESE region there is the gas with a line-of-sight velocity of about 1700 km/s; it is larger by 300 km/s than the systemic velocity of the galaxy. The gas with the similar velocity is observed at the southwestern edge of the gaseous disk according to the Fabry-Perot velocity field (Silchenko et al., 2019), and this velocity does not match any

circular rotation models. Apparently, as regarding the ESE clump, this may be a compact remnant of a satellite which has hit the NGC 2655 disk with a high impact velocity of 400–500 km/s almost at a right angle to the stellar disk. The whole configuration with a destroyed companion and a polar circumnuclear loop looks like the destroyed Milky Way companion dSgr stretched into a polar stream in our Galaxy (Ibata et al., 2001; Laporte et al., 2018). And the NGC 2655 proper gas, which was hit in the center by the fallen companion, should have lost momentum in the shock wave and inflow into the nucleus; perhaps, this is what fuelled the current activity of the nucleus.

5 DISCUSSION

5.1 Structure and Stellar Kinematics of NGC 2655

NGC 2655 is a giant early-type disk galaxy. It is commonly accepted that such galaxies should have a very large dominant bulge. Indeed, a detailed morphological analysis and decomposition of the galaxy image into components undertaken as a part of the S4G survey of galaxies (Sheth et al., 2010) showed that the disk contributes no more than 42% to the near-infrared luminosity – and then to the stellar mass (Salo et al., 2015). According to this decomposition, the exponential disk starts to dominate in the surface brightness at the radii of $R > 50''$, while closer to the center, the surface brightness profile represents a combined contribution of the bulge and bar. Why have the Salo et al. (2015) team decided that NGC 2655 has a bar, even though the galaxy is not classified as SB in any catalog? This is due to the fact that the major-axis orientation of the isophotes of the inner components – the one with the $PA_1 = 82^\circ$, and the other with $PA_2 = 85.6^\circ$, – differ from the orientation of the outermost disk isophotes, $PA_0 = 110^\circ$, which is commonly treated as the orientation of the line of nodes (under the assumption of the round intrinsic shape of the disk). As a result, the NGC 2655 image deprojection undertaken in the S4G survey by the Salo et al. (2015) team exactly with this line-of-nodes orientation,

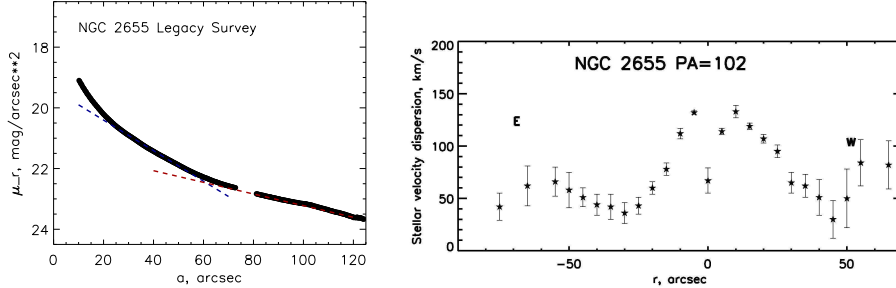


Figure 7: The azimuthally-averaged surface-brightness profile of NGC 2655, according to the BASS survey data (taken from Legacy Survey, Dey et al. 2019), fitted by two exponential segments, $\mu_r = 19.4 + 1.086R''/21.6''$, in the radius range of $R = 26'' - 50''$, and $\mu_r = 21.3 + 1.086R''/56.5''$, in the radius range of $R = 70'' - 120''$ (*the left plot*), and the LOS stellar velocity dispersion profile in the $PA = 102^\circ$ cross-section, according to the long-slit data (*right*).

$PA = 110^\circ$, has given the intrinsic galaxy shape with the oval inner components; the Salo et al. (2015) team considered one of them as a triaxial bulge, and the other as a bar.

We do not agree with this interpretation of the structure of NGC 2655. The fact is that the stellar LOS velocity field obtained for the central part of the galaxy with the SAURON IFU looks like a regular circular rotation (Dumas et al., 2007). We analyzed this velocity field using the tilted ring method and found the line-of-nodes orientation for the stellar-component rotation plane $PA = 263^\circ \pm 3^\circ$ up to the distance of $25''$ from the center. Dumas et al. (2007) obtained with the kinemetry method $PA = 266^\circ \pm 1^\circ$ using the same data. The exact coincidence of the orientations of the photometric and kinematical major axes proves that the stars in the center of NGC 2655 rotate in circular orbits within the axisymmetric potential: the galaxy has no bar.

Another important diagnostic feature of a thin stellar disk is that it must be dynamically cold: its rotation velocity must be several times greater than the stellar velocity dispersion. Figure 7, right, shows the profile of stellar velocity dispersion that we measured along the cross section with a long slit at $PA = 102^\circ$. The stellar line-of-sight velocities and velocity dispersions were measured by the cross-correlation method similar to that we used in the paper

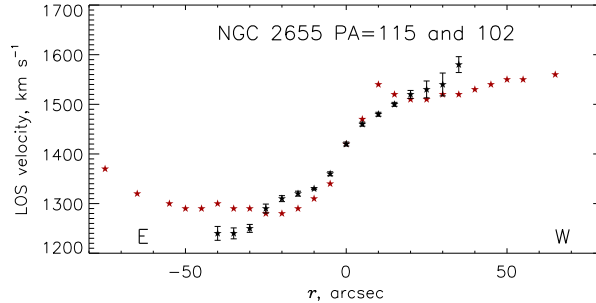


Figure 8: The stellar LOS velocity profiles along two long-slit cross-sections close to the photometric major axis: the red stars are for $PA = 102^\circ$, and the black stars – for $PA = 115^\circ$.

by Silchenko et al. (2019). Already at the radius of $R = 30''$, the stellar velocity dispersion drops to 50 km/s: this is the radial boundary, where the thin stellar disk begins to dominate. We have also shown in Fig. 7, left, the decomposition of the surface brightness profile consistent with the dominance of the disk so close to the center: the photometric disk of NGC 2655 has the type III profile, that is, it consists of two exponential segments, the inner one with a smaller scalelength than the outer (which was also found in the S4G survey).

Thus, we can state that NGC 2655 has two exponential disks: they have different scalelengths, but they also have different orientations of the isophote major axis. And along with this, the orientation of the major axis of the inner isophote is supported by the stellar kinematics: as the analysis of the two-dimensional velocity field shows, this is indeed the line of nodes of the circular rotation plane. As for the outer disk, for which the orientation of the photometric major axis $PA = 110^\circ$ was found in the S4G survey, here we cannot properly compare it with the orientation of the kinematical major axis: there is no two-dimensional stellar velocity field over a large extension, $R > 20''$, of the galaxy disk. But we have long-slit cross-sections in different slit orientations. Figure 8 compares the line-of-sight velocity profiles for the stellar component in the slit orientations $PA = 102^\circ$ and $PA = 115^\circ$. We can note that at the radius of $R = 40''$ the rotation velocity projected onto the line of sight in $PA = 115^\circ$ is larger than that in $PA = 102^\circ$. This means that the kinematical major axis in the outer stellar disk is

closer to $PA = 115^\circ$ than to $PA = 102^\circ$ which excludes the line-of-nodes orientation found for the inner stellar component. At the same time, the photometric major-axis orientation of the outer disk may be the orientation of the line of nodes: our kinematical cross-sections with a long slit do not exclude this. It appears that the internal and external rotation axes of the stellar disk of NGC 2655 are inclined to each other, in other words, NGC 2655 is a multi-spin galaxy.

5.2 The Origin of Gas in NGC 2655

The orientations of the huge disk of neutral hydrogen and the outer stellar disk in NGC 2655 coincide with each other both spatially and kinematically. Previously, Sparke et al. (2008) noted that two billion solar masses of cold gas is too much for one minor merger, and several such events are needed (but with the same orientation of the infall orbits, because all the gas rotates in the same plane). Now we understand that these multiple minor mergers should have brought not only several billion solar masses of gas, but also several billion solar masses of stars for the outer stellar disk of NGC 2655, which makes the supposed multiple minor merging a quite incredible event. Opposite to Sparke et al. (2008), we conclude that the outer gaseous disk lies within the outer stellar disk, and even current star formation is taking place somewhere in it: it is at the southern edge of the disk that we have detected the gas emission excited by young stars, and the northern arc shows also an excess of ultraviolet (Fig. 4). The metallicity of the gas in this outer disk is solar, which is atypical for dwarf galaxies that Sparke et al. (2008) have suggested as the source of NGC 2655 gaseous disk. The entire external configuration of the galaxy resembles a classical large disk of a spiral galaxy, which, according to modern evolution concepts, is cumulated over billions years by smooth external accretion of cold gas (Tacconi et al., 2020), albeit from a source undefined still at a global scale.

But minor merging certainly took place in NGC 2655. It also brought along a noticeable amount of the gas with the spin strongly decoupled from the regular rotation of the outer

disk, both stellar and gaseous. Apparently, a companion fell onto the galaxy almost vertically, and now, within two kiloparsecs from the center, we observe the remnants of the destroyed companion as a circumpolar loop – the picture is very similar to Sagittarius dwarf torn apart by the Milky Way. But in the case of NGC 2655, there was much more gas in the merged companion. The gas of the vertically infalling companion hit the gaseous disk of NGC 2655 being in regular rotation, and this collision inevitably resulted in the development of shock fronts. The shock wave has not only excited the gas in the polar loop, it ran outward across the large galactic gaseous disk. At distances of up to 8 kpc from the center, we observe the gas of the large disk excited by this shock wave, although, the kinematics of this gas to the east of the nucleus is little affected and exhibits rotation consistent with that of the stellar disk. If the shock wave propagated at an average velocity of 1000 km/s, then the impact could have taken place approximately 10^7 years ago.

6 ACKNOWLEDGMENTS

The paper is based on the observational data obtained with the 6-m telescope at the Special Astrophysical Observatory of the Russian Academy of Sciences (BTA SAO RAS) and with the 2.5-m telescope at the Caucasus Mountain Observatory of the Sternberg Astronomical Institute of the Moscow State University. The spectroscopic analysis was supported by the grant of the Russian Science Foundation no.22-12-00080, and the narrow-band photometry – by the grant of the Russian Fund for Basic Research no. 20-02-00080. The observations at the BTA SAO RAS telescope are supported by the Ministry of Science and Higher Education of the Russian Federation; the observational technique is improved in the frame of the National project "Science and universities". In our analysis we used data from publicly accessible archives and databases: the Lyon-Meudon Extragalactic Database (LEDA) maintained by the LEDA team at the Lyon Observatory CRAL (France) and the NASA/IPAC Extragalactic Database (NED) operated by the Jet Propulsion Laboratory of the California Institute of Technology under

contract with the National Aeronautics and Space Administration (USA). We also invoked the data from the GALEX space telescope for our analysis. The NASA GALEX data were taken from the Mikulski Archive for Space Telescopes (MAST). In our figures we have also used the plots provided by observations made with the NASA/ESA Hubble Space Telescope and obtained from the Hubble Legacy Archive, which is a collaboration between the Space Telescope Science Institute (STScI/NASA), the Space Telescope European Coordinating Facility (ST-ECF/ESA) and the Canadian Astronomy Data Centre (CADC/NRC/CSA). The broad-band photometry is based on the data taken from the Legacy Survey resource (the BASS survey). The Legacy Surveys consist of three individual and complementary projects: the Dark Energy Camera Legacy Survey (DECaLS; Proposal ID no.2014B-0404; PIs: David Schlegel and Arjun Dey), the Beijing-Arizona Sky Survey (BASS; NOAO Prop. ID no.2015A-0801; PIs: Zhou Xu and Xiaohui Fan), and the Mayall z-band Legacy Survey (MzLS; Prop. ID no.2016A-0453; PI: Arjun Dey). BASS is a key project of the Telescope Access Program (TAP), which has been funded by the National Astronomical Observatories of China, the Chinese Academy of Sciences (the Strategic Priority Research Programs, Grant no. XDB09000000), and the Special Fund for Astronomy from the Ministry of Finance. The BASS is also supported by the External Cooperation Program of Chinese Academy of Sciences (Grant no. 114A11KYSB20160057), and Chinese National Natural Science Foundation (Grant no. 12120101003, no. 11433005).

References

- [1] V. L. Afanasiev and A. V. Moiseev, *Baltic Astronomy* **20**, 363 (2011).
- [2] M. G. Allen, B. A. Groves, M. A. Dopita, et al., *ApJ Suppl. Ser.* **178**, 20 (2008).
- [3] J. A. Baldwin, M. M. Phillips, R. Terlevich, *PASP* **93**, 5 (1981).

- [4] A. Y. K. Bouquin, A. Gil de Paz, J. C. Munoz-Mateos, et al., *ApJ Suppl. Ser.* **234**, Aid.18 (2018).
- [5] B. Catinella, A. Saintonge, S. Janowiecki, et al., *MNRAS* **476**, 875 (2018).
- [6] L. Cortese, B. Catinella, R. H. W. Cook, et al., *MNRAS* **494**, L42 (2020).
- [7] T. A. Davis, K. Alatalo, M. Sarzi, et al., *MNRAS* **417**, 882 (2011).
- [8] A. Dey, D. J. Schlegel, D. Lang, et al., *AJ* **157**, Aid.168 (2019).
- [9] G. Dumas, C. G. Mundell, E. Emsellem, N. M. Nagar, *MNRAS* **379**, 1249 (2007).
- [10] A. M. Garcia, *Astron. Astrophys. Suppl.* **100**, 47 (1993).
- [11] M. Grossi, S. di Serego Alighieri, C. Giovanardi, et al., *A& A* **498**, 407 (2009).
- [12] J. E. Gunn and J. R. Gott, III, *ApJ* **176**, 1 (1972).
- [13] L. C. Ho and J. S. Ulvestad, *ApJ Suppl. Ser.* **133**, 77 (2001).
- [14] E. P. Hubble, *The Realm of the Nebulae*. (Yale Univ. Press: New Haven, 1936).
- [15] W. K. Huchtmeier and O. G. Richter, *A& A* **109**, 331 (1982).
- [16] E. Hummel, J. M. van der Hulst, J. M. Dickey, *A& A* **134**, 207 (1984).
- [17] R. Ibata, M. Irwin, G. F. Lewis, A. Stolte, *ApJ* **547**, L133 (2001).
- [18] I. Yu. Katkov, A. Yu. Kniazev, O. K. Silchenko, *AJ* **150**, Aid.24 (2015).
- [19] G. Kauffmann, T. M. Heckman, Ch. Tremonti, et al., *MNRAS* **346**, 1055 (2003).
- [20] W. C. Keel and E. Hummel, *A& A* **194**, 90 (1988).

- [21] L. J. Kewley, M. A. Dopita, R. S. Sutherland, et al., *ApJ* **556**, 121 (2001).
- [22] K. Kuijken, D. Fisher, M. R. Merrifield, *MNRAS* **283**, 543 (1996).
- [23] C. F. P. Laporte, K. V. Johnston, F. A. Gómez, et al., *MNRAS* **481**, 286 (2018).
- [24] R. B. Larson, B. M. Tinsley, C. N. Caldwell, *ApJ* **237**, 692 (1980).
- [25] B. M. Lewis and R. D. Davies, *MNRAS* **165**, 213 (1973).
- [26] R. A. Marino, F. F. Rosales-Ortega, S. F. Sánchez, et al., *A& A* **559**, A114 (2013).
- [27] A. V. Moiseev and O. V. Egorov, *Astrophys. Bull.* **63**, 181 (2008).
- [28] M. Pettini and B. E. J. Pagel, *MNRAS* **348**, L59 (2004).
- [29] H. Salo, E. Laurikainen, J. Laine, et al., *ApJ Suppl. Ser.* **219**, Aid.4 (2015).
- [30] P. Serra, T. Oosterloo, R. Morganti, et al., *MNRAS* **422**, 1835 (2012).
- [31] W. W. Shane and N. Krumm, *IAU Symp.* **100**, 105 (1983).
- [32] N. Shatsky, A. Belinski, A. Dodin, et al., In *Proc. of Conf. on Ground-Based Astronomy in Russia. 21st Century*, Nizhny Arkhyz, Russia, 2020, pp.127–132.
- [33] K. Sheth, M. Regan, J. L. Hinz, et al., *PASP* **122**, 1397 (2010).
- [34] O. K. Silchenko and V. L. Afanasiev, *AJ* **127**, 2641 (2004).
- [35] O. K. Silchenko and A. N. Burenkov, *A& A* **233**, 314 (1990).
- [36] O. K. Silchenko, A. V. Moiseev, and O. V. Egorov, *ApJ Suppl. Ser.* **244**, Aid. 6 (2019).
- [37] L. S. Sparke, G. van Moorsel, P. Erwin, E. M. H. Wehner, *AJ* **135**, 99 (2008).

- [38] L. J. Tacconi, R. Genzel, A. Sternberg, *Annual Review Astron. Astrophys.* **58**, 157 (2020).
- [39] Y. Terashima, N. Iyomoto, L. C. Ho, A. F. Ptak, *ApJ Suppl. Ser.* **139**, 1 (2002).